Journal of the Korean Society of Oceanography
Vol. 34, No. 4, pp. 185—199 December 1999

A Numerical Experiment on the Dispersion of the Changjiang River Plume

INKWEON BANG AND HEUNG-JAE LIE
Physical Oceanography Division, Korea Ocean Research and Development Institute
Ansan P.O. Box 29, Seoul 425-600, Korea

With a realistic geography and topography the Princeton Ocean Model is used to study the effects of topography, wind and time-varying Changjiang (Yangtze) River discharge on the dispersion of the Changjiang River plume in the Yellow and East China Seas. The topographic feature of deepening offshore suppresses the offshore expansion of the discharged low salinity water while spreading along the coast is not hindered. Also the spreading of the Changjiang River plume is very sensitive to wind conditions and the southerly wind is most responsible for the eastward expansion toward the Cheju Island. It is also shown that the influence of the Changjiang River Diluted Water on the hydrography and circulation of the Yellow Sea including the South Sea of Korea is substantial even in the absence of tide, wind and current.

INTRODUCTION

The Changjiang River originates from the Tibetan Plateau and empties to the East China Sea. Its length is 6,300 km and in the middle of the Changjiang River Three Gorges Dam is now under construction with the scheduled completion year of 2009. The freshwater discharge of the Changjiang River is the third largest in the world after the Amazon River and the Congo River. The annual discharge is 900 km^3 and it corresponds to about 32 times that of the Aprok River and 18 times that of the Yellow River (Hong *et al.*, 1995). Therefore, this huge amount of freshwater discharge would influence not only on the ocean environment and circulation in the East China Sea but also those in the Yellow Sea. Furthermore, as the construction of the Three Gorges Dam is expected to cause big changes in the East China and Yellow Seas, prediction studies on the possible changes as well as data gathering prior to the construction are absolutely necessary.

In July and August, 1998 there were lots of losses in the properties and lives in China due to heavy rains and flooding. A record-high water levels were observed and we may therefore assume that the discharge was about the same as that in August 1954 when the largest monthly mean discharge of 84,000 m^3/s was observed (Shen *et al.*, 1998). Observation data in Shen *et al.* (1998) are from the Datong Station located 640 km upstream from the river mouth and the annual mean discharge over 36 years (1950—1985) is 28,400 m^3/s.

The behavior of the Changjiang River Diluted Water (hereafter CRDW) shows seasonal variations. Observations showed that in winter the outflow of the Changjiang River flows southward along the coast but in summer it directs to the northeast toward the Cheju Island (see Fig. 6 in Hu, 1994). Low salinity water which appears in summer occasionally near the Cheju Island and causes annihilation of the fish and bivalves is suspected to originate from the CRDW. The low salinity water spotted even in the East Sea is suspected to originate from CRDW with the trajectories of the recent drifter experiments (Lie *et al.*, 1998). The turning of the outflow to the right (southward) in winter is due to the Coriolis effect. However, the northeastward turning in summer requires other dynamical explanations and many efforts have been attempted to explain it (Guan, 1994; Mao *et al.*, 1963; Cao, 1980; Le, 1984; Yuan *et al.*, 1982; Hu, 1994).

Guan (1994) considered the fluctuation of the Changjiang River discharge as one of the major factors controlling the dimension and direction of the CRDW. He also listed the seaward deepening of the bottom, boundary effect of the Taiwan Warm Current, southerly wind and baroclinic effects as possible factors influencing the northeastward turning. Importance of the lateral mixing is also mentioned by many researchers (Mao *et al.*, 1963; Cao, 1980; Le, 1984; Yuan *et al.*, 1982). Hu (1994) concluded that the wind

is the major factor for the turning, *i.e.* the southerly wind is dominant in summer and the current is northward or northeastward from the coast to the offshore (the Kuroshio and its branches are also responsible for this). He noticed also that when wind collapses or reverses either in winter or in summer for a certain period of time, the plume turns right in summer or turns left in winter.

There have not been many numerical modeling studies about the detailed extent and range of the CRDW. Most numerical modeling studies on the ocean circulation in the Yellow and East China Seas considered the discharge of the Changjiang River as one of the boundary condition. Yuan and Su (1984) used a steady-state barotropic model and time-dependent two-layer model with poor resolution of 1°. For the discharge amounting to 34,000 m^3/s, the resulting plume was shown to be advected with the northward flowing Taiwan Current and blocked by the Yellow Sea Bottom Cold Water. Lee (1996) and Zhu and Shen (1996) simulated the winter and summer circulations in the Yellow and East China Seas using 3-dimensional numerical models. Recently, Lee (1999) included M_2 tide as well as the wind and the Kuroshio in the simulation of the time-varying circulation. However, in these studies river discharge from the Changjiang River was one of the many forcings that its individual effect could not be evaluated properly.

A coastal current is established along the coast on the right hand side of the river in the northern hemisphere after the passage of Kelvin wave (McCreary *et al.*, 1997). If the flow is nonlinear, an anticyclonic gyre is formed at the river mouth and the river outflow is bypassed through this gyre to feed the coastal current. However, this circulation pattern will be greatly altered if other effects are included such as topography, wind, mean current, tide. Furthermore, it is not easy to isolate the effects of individual forces if all of these external forces are present at the same time. Therefore, in this study we start from the very simple experiment and add factors one by one to the model to assess their individual impact on the ocean circulation in the Yellow and East China Seas.

Firstly, we are considering the effect of topography on the northeastward turning of the CRDW. It is studied by comparing the results with those of a control experiment which has a flat bottom. Secondly, effect of the wind on the dispersion of CRDW are discussed. The last experiment is performed by employing fluctuations in the Changjiang River discharge and we run the model for a period of two years. This experiment is aimed to examine the dispersion pattern of the CRDW and time required to reach Korea in the absence of any other external forces. The model experiments are unrealistic but they clearly show the importance of the CRDW both in the ocean circulation and in the ocean environment in the Yellow and East China Seas.

NUMERICAL MODEL

Princeton Ocean Model (POM) which is formulated in sigma coordinate system is used for this study and detailed model descriptions are given in Mellor (1996). Mellor and Yamada (1982) 2.5-level turbulence closure scheme is implemented for the calculation of the vertical eddy coefficients. The horizontal eddy coefficients are parameterized using the Smagorinsky diffusion formula

$$A=C\Delta x\Delta y\sqrt{(\partial u/\partial x)^2+(\partial v/\partial y)^2+\frac{1}{2}(\partial v/\partial x+\partial u/\partial y)^2}$$

where Δx, Δy is the horizontal grid size and C is a constant taken to be 0.2.

Model domain consists of 139×249 horizontal grids with 5'×3.75' grid spacing and spans the area of about 21°—37°N, 119°—130°E. Topography data compiled by KORDI (1997a) are used but maximum depth is set to 500 m. Since water depth increases to the east we set the depths at all grid points east of the first grid point where the water depth is greater than 500 m along each latitude line. This is done to avoid possible numerical instability in the region of sudden depth changes. Also depths at the grid points south of the 50th grid point are set equal to the depth at the 50th grid point (Fig. 1). Regions of these artificial treatments are far from the river mouth and are located in the downstream region that the solution is not expected to be affected. Integration time interval is 20 seconds for the external mode and 10 minutes for the internal mode. In vertical direction there are 10 layers (the layer is defined here as the water column between levels and the top and bottom levels correspond to the sea surface and the bottom, respectively) and the depths to the center of each layer (water depth is 20 m) are listed in Table 1. The Coriolis parameter varies with latitude and all boundaries are closed except the east and south boundaries where a radiating boundary condition is used.

Four y-grid points of 162—165 corresponds to the mouth of the Changjiang River and the width is about 28 km (Fig. 2). The river mouth is located at 35th

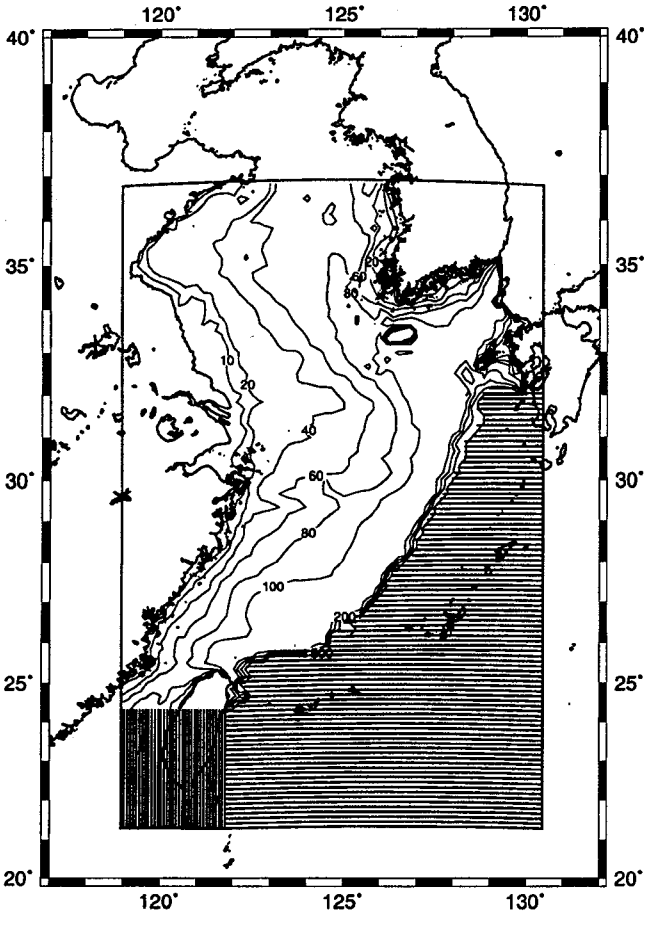

Fig. 1. The rectangular box shows the model region. Model is closed across the Korea Strait and along the Ryukyu Islands. Depth in the horizontally hatched area is 500 m and meridional depth change is zero in the vertically hatched area (isobath intervals are 20 m to 100 m and 100 m to 500 m. Isobath of 10 m is also shown).

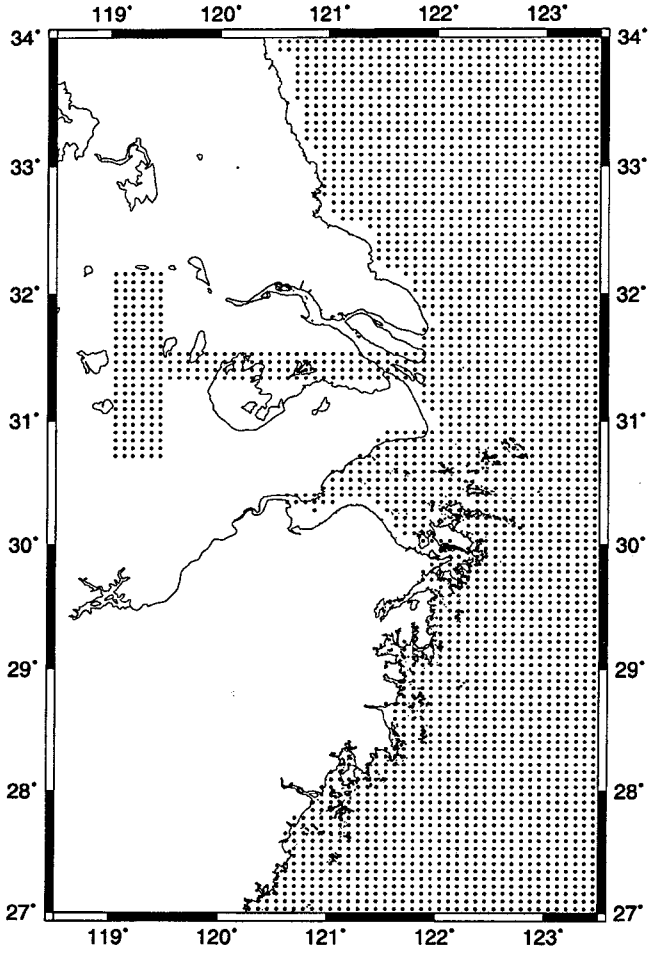

Fig. 2. Grid points near the Changjiang River. The model Changjiang River consists of a reservoir and a long channel.

x-grid point and its width is maintained to the 7th x-grid point. The Changjiang River estuary has two branches, North Branch (NB) and South Branch (SB) and net flow through the NB is practically zero (Kangshan *et al.* 1983). SB again is divided into two passages by the presence of the Changxing Island, North Passage (NP) and South Passage (SP). NP carries 2/3 of the total discharge and SP the rest. The combined width of NP and SP is about 20 km at the river mouth and is about one grid point smaller than the model river mouth but we do not expect the resulting change to be large.

SP again is divided into two channels, North Channel (NC) and South Channel (SC). Net discharge through SC averaged over a tidal cycle is negative, *i.e.* landward and therefore all the discharge through SP occurs through NC (Kangshan *et al.*, 1983). The Changjiang River near the river mouth is oriented to the southeast, but NP and NC of SP where most of the discharge flows is more or less oriented to the east-southeast (ESE). Also, observations in summer shows that the outflow have a stronger eastward component than the southward component (Kangshan *et al.*, 1983). Thus, the model river mouth may represents the orientation of the Changjiang River properly.

The model river mouth is connected to a freshwater reservoir with 24 y-grid points wide and 6 x-grid

Table 1. Depths to the center of each layer

Layer	1	2	3	4	5	6	7	8	9	10
Depth (m)	0.18	0.50	1.02	2.02	4.28	7.14	10.00	12.86	15.72	18.58

points long. Such freshwater reservoir is also employed in Oey and Mellor (1993) and this approach mitigates the need to prescribe boundary condition at the river mouth which usually takes the form of the two-layer estuarine circulation (for example, see Chao, 1988). The magnitude of discharge is controlled by setting the vertically averaged velocity over the west wall of the freshwater reservoir to a prescribed value. Salinity values are set to zero at all vertical layers of the west 30 grid points at every timestep.

RESULTS

Constant discharge experiment

In this experiment a constant velocity is given at the west wall of the freshwater reservoir to produce a constant discharge of about 80,000 m^3/s which presumably corresponds to the magnitude in summer, 1998. To find out the effect of topography, two cases, one with a flat bottom and the other with a realistic topography, are integrated for 100 days. The flat bottom case has a water depth of 20 m everywhere and the prescribed velocity is 5 cm/s. In the realistic topography case the prescribed velocity is increased to 10 cm/s to compensate for the shallower water depth at the river mouth. Discharge at the river mouth is monitored during the whole integration period (Fig. 3a). Initially the model ocean and river are filled with motionless waters of constant salinity of 35 psu (temperature is excluded in the computation).

In the flat bottom case the discharge jumps to about 80,000 m^3/s within one day and shows oscillations with almost equal period and amplitude. In Fig. 4 salinity distributions in the first layer are shown at 20-day interval for both the flat bottom and realistic topography cases. In this study the 34 psu isopleths are considered as the boundary of the low salinity plume. An anticyclonic gyre near the river mouth and a coastal current along the south coast are formed as in the channel experiment of KORDI (1997b). The coastal current reaches the Taiwan Strait (~25°N) after 40 days of integration with the propagation speed of about 19 cm/s. This speed is less than 23 cm/s of the channel experiment (KORDI, 1997b).

The offshore boundary of the coastal current remains stable until day 20 but it becomes unstable from day 30 and a wavelike structure is being developed. The boundary becomes more unstable with time and

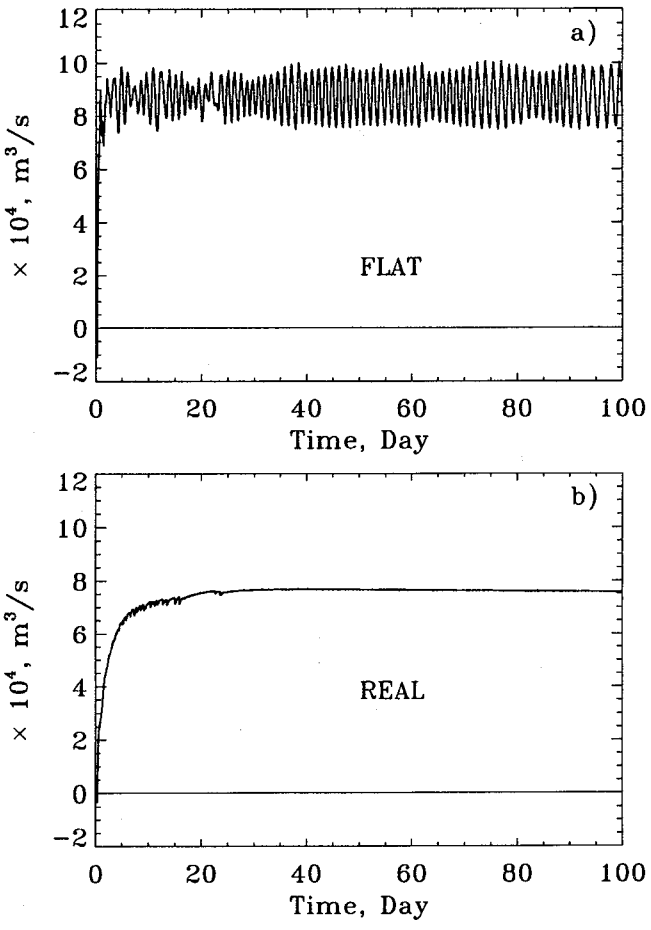

Fig. 3. Time variation of discharge at the river mouth for (a) flat bottom and (b) realistic topography case.

the coastal current becomes wider. At day 80 the low salinity plume arrives at the Taiwan Strait and surrounds the whole Taiwan at day 100. As a result the coastal current is wider than the bulge near the river mouth.

In the realistic topography case the discharge increases slowly as compared with the flat bottom case and the magnitude larger than 70,000 m^3/s is reached after 10 days of integration. Unlike the flat bottom case there are no significant oscillations. (Fig. 3b). Salinity distributions are similar to the flat bottom case but there are also differences (Fig. 4). The plume is shifted further north, the offshore expansion is less, and the coastal current is less unstable. All these differences are caused by the introduction of the topography and the east-west depth gradient is especially thought to play a major role. The water depth deepens to the east and therefore the isobaths are oriented along the north-south direction. The isobaths are lines of the equal potential vorticity that the east-west movement of the water column would be difficult

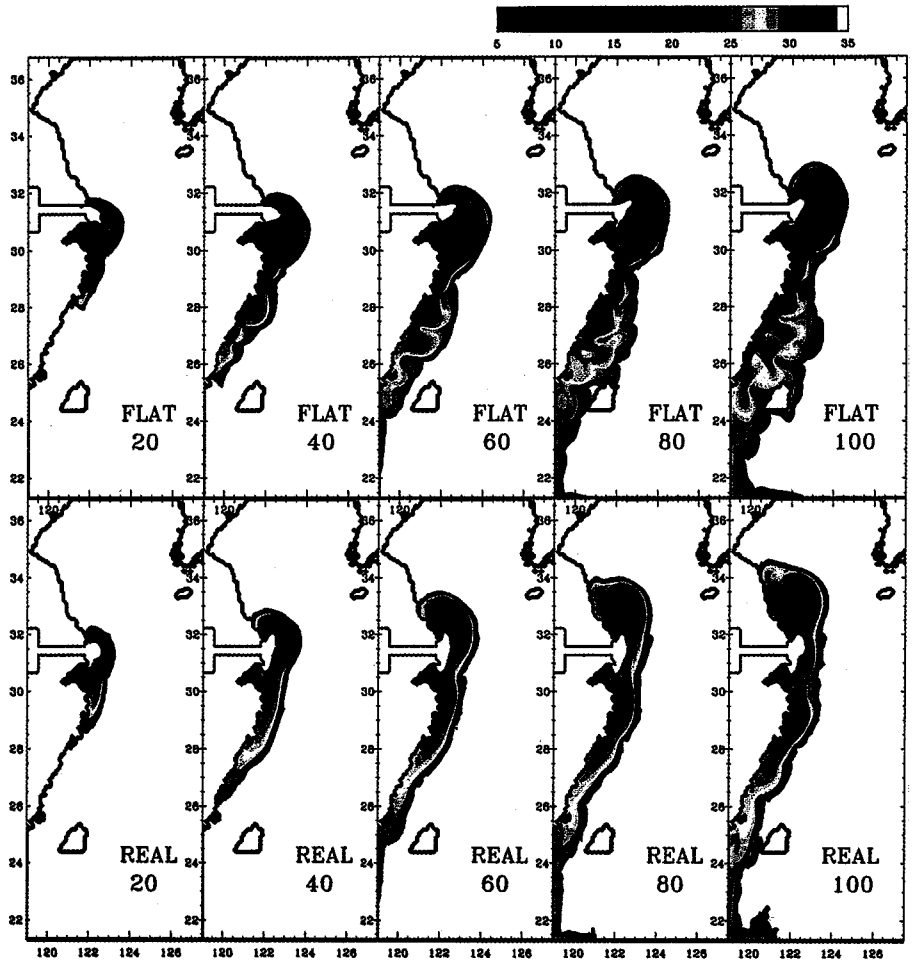

Fig. 4. Salinity distributions in the 1st layer at 20-day interval for the flat bottom (upper) and realistic topography (lower) cases (thick line indicates 30 psu).

while the north-south movement is rather easy. As a result, the coastal current becomes stable and the offshore expansion is reduced. The northward shift of the plume could be due to the positive vorticity induced by the stretching as the water column enters the deeper region from the shallower region. Or, it could be explained in terms of the coastally trapped solution of McCreary *et al.* (1997) in that a northward current along the north coast is formed as a compensating flow of the southward current along the offshore front.

The coastal current along the south coast reaches the Taiwan Strait after 100 days of integration, 20 days later than the flat bottom case. The width of the coastal current remains fairly constant at about 100 km with a slight increase with time. At day 100 the northward plume reaches 34.5°N and the maximum offshore expansion, about 300 km wide, occurs at locations north of the river mouth. Current distributions in the first layer at days 50 and 100 are shown in Figs. 5 and 6. The river flow initiated in the freshwater reservoir exits the river with a small northward excursion, but it soon flows southward. On the contrary, waters at the grid points north of the river mouth flow to the north or northeast. At day 50, flows exiting through the southern two grid points in the river mouth change the direction to the south right after exit. But flows through the northern two grids turn first to the northeast and gradual change in the clockwise direction occurs after flowing some distance. It finally joins the southward flow.

Offshore of this local flow structure there exist a large scale anticyclonic gyre as is also shown in the salinity distribution. A northward flow is formed north of the river mouth along the coast. At the northern tip of the flow it turns clockwise and then heads to the south. The southward flow continues to the latitudes of the river mouth and changes its direction to southwest to become the coastal current along the south coast. At day 100 the waters flowing through the southern two grid points in the river mouth turn immediately to the south like at day 50, but the waters through the northern two grid points join the southward flow of the large-scale gyre. The north-

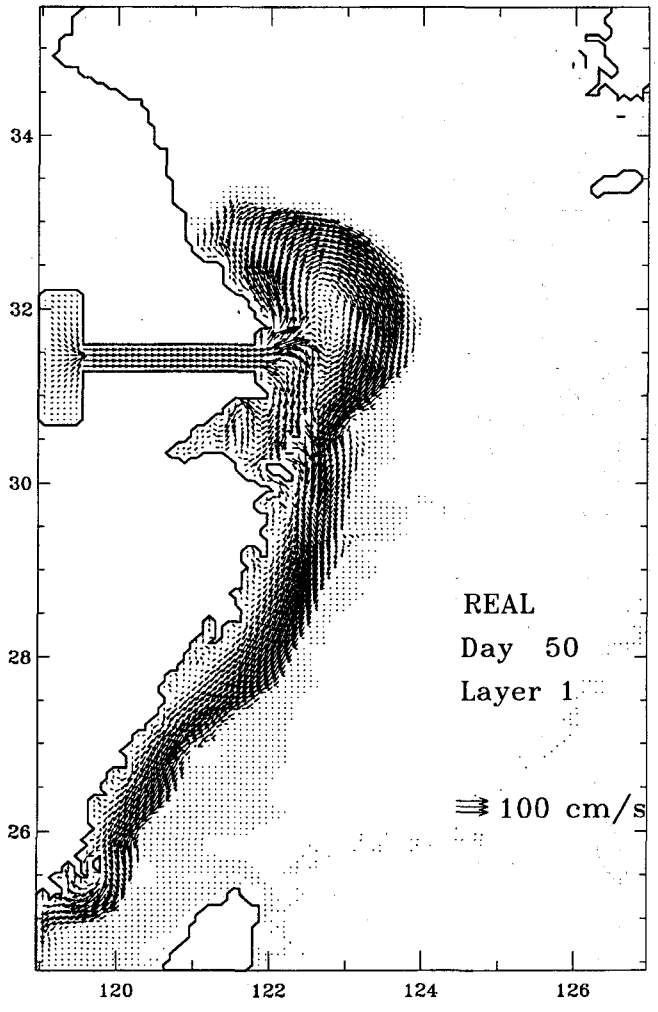

Fig. 5. Velocity distribution in the 1st layer at day 50 for the realistic topography.

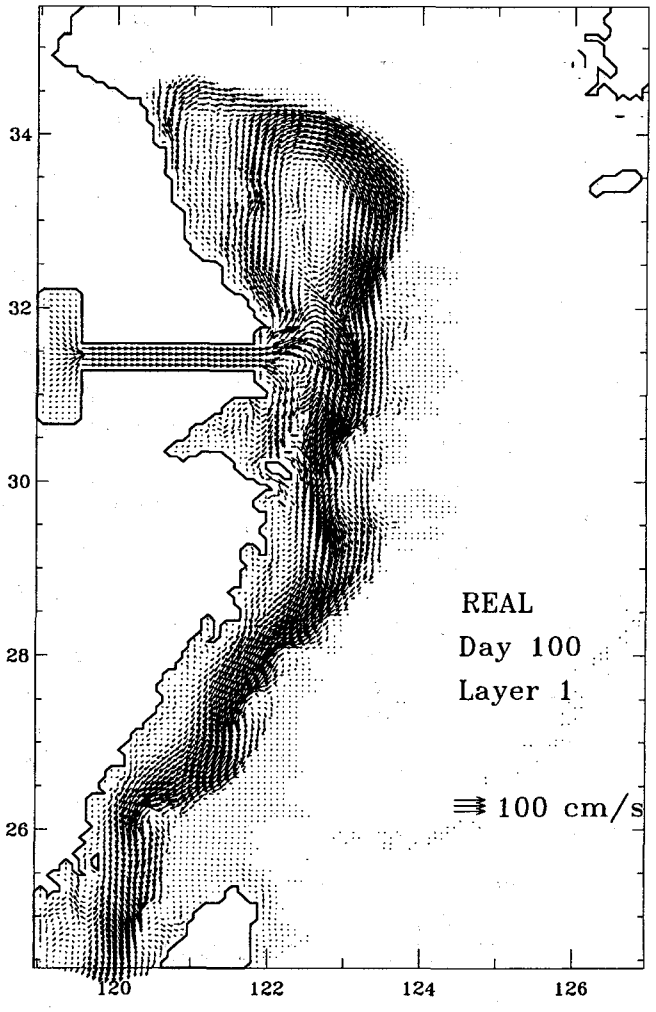

Fig. 6. Same as Fig. 6, but at day 100.

ward current north of the river mouth flows along the coast before it leaves the coast at 32.5°N and continues to flow northward. Near the coast at 34°N a remnant of the old northward flow that existed before day 100 is seen. The northward flow separated from the coast forms a gyre like at day 50 but the location is shifted to the north, i.e. at day 50 the anticyclonic gyre is present around the river mouth, but at day 100 the gyre is shifted to the north and a new gyre is about to be formed near the river mouth. However, formation of a circular shape gyre would not be possible because of the changes in the background state. At the beginning there was no background stratification and therefore no background current, but now the presence of the low salinity waters make the flow structure very complicated that the formation of the circular shape gyre would be challenged at each moment by the current.

Figs. 5 and 6 are the flow distributions at the sigma levels that the current vector cannot be considered to represent the flow path since the water depths at each grid point are different for the realistic topography case. Therefore we interpolated velocities from the sigma-level to the z-level to obtain velocities at a constant depth and current vectors at water depth of 5, 10, 30 m are shown for day 50 (Fig. 7). In the interpolation, sea level variations are ignored because it is much less than the water depth.

At 2 m depth the flow distribution has almost the same pattern as in the sigma coordinate system with only one noticeable difference; more waters seem to flow northward near the river mouth (not shown). At 5 m depth there is almost no southward flow at the river mouth and all the waters coming out of the river flow to the north and form an anticyclonic gyre. Most of the southward flow in the right half of the gyre continues to the coastal current along the south coast and a small portion flows westward to join the northward outflow from the river. At 10 m depth the

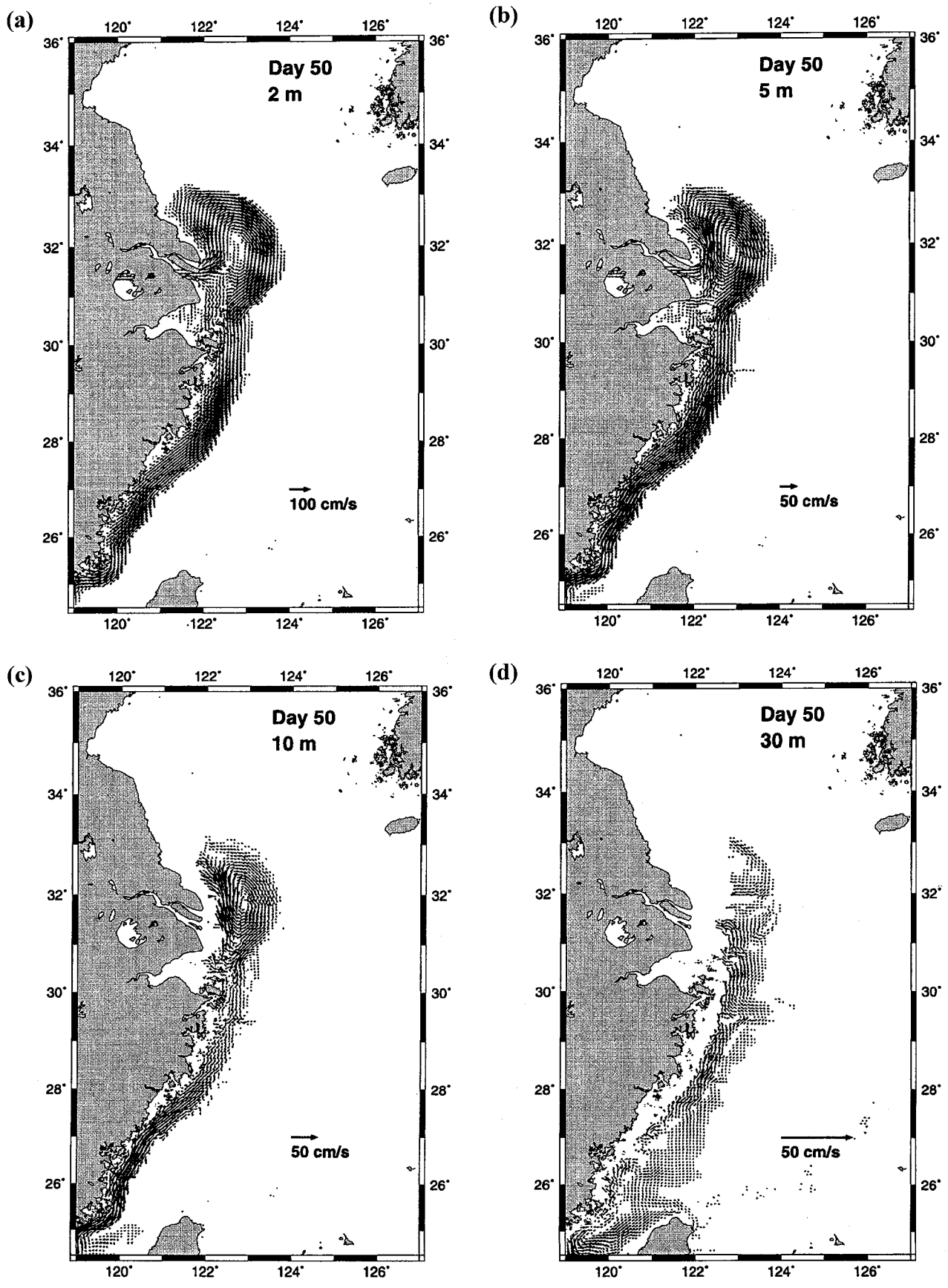

Fig. 7. Velocity distribution at depths of 2, 5, 10, 30 m at day 50 for realistic topography case.

flow has no direct connection with the river (the water depth at the river mouth is 7 m), but there still exist a similar anticyclonic gyre and coastal current as in the shallow depths. At 30 m depth, however, the anticyclonic gyre disappears and a northward flow is developed along the coast where a southward flowing coastal current exists at shallower depths. There is also onshore flow near the river mouth.

Wind experiment

In this experiment we examine the effects of the wind on the distribution of the low salinity water. The end state of the previous experiment, *i.e.* day 100 is the starting point in this experiment. Wind with magnitude of 0.5 dyne/cm^2 are applied for 10 days. To reduce the shock by the sudden introduction of the wind it has been ramped up linearly over 1 day. Four different wind directions are applied and salinity distributions in the first layer are shown at 2-day interval. First, upper panel of Fig. 8 is for the westerly case and it shows that the low salinity region has expanded to the south, *i.e.* the water is transported to the right of the applied wind stress as expected by Ekman dynamics. This Ekman response is clear in all cases. The low salinity plume is advected to the north in the easterly case (lower panel of Fig. 8) and to the west toward the Chinese coast in the northerly case (Fig. 9).

When the wind blows from south the plume is advected to the east, *i.e.* to the offshore direction and reaches the Cheju Island (lower panel of Fig. 9). This clearly suggests a possibility that the low salinity water that appears in summer near the Cheju Island may be the CRDW advected by the southerly wind, predominant in summer. Of course, other factors such as current and tide can affect the situation. But this experiment clearly shows that the wind effects on the dispersion of the CRDW are big and the ocean response to the wind is fast.

Fig. 10 shows changes in the salinity by the introduction of the southerly wind, *i.e.* difference of the salinity between the southerly case and no wind case.

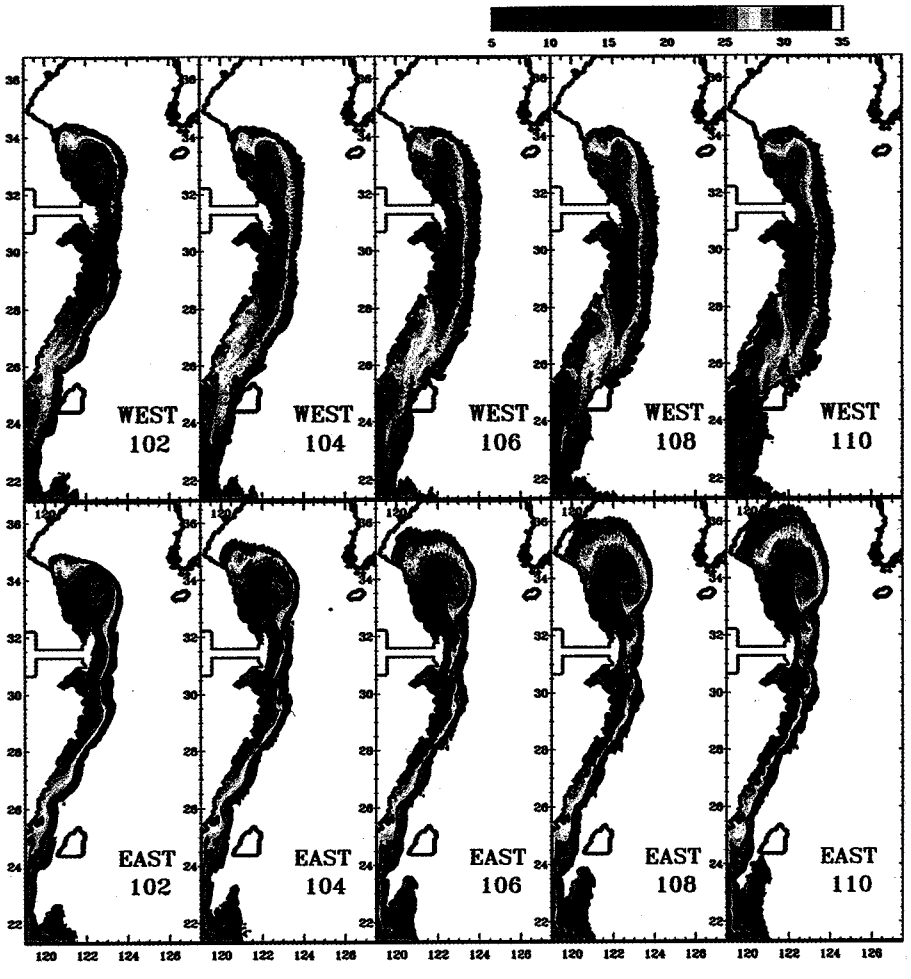

Fig. 8. Salinity distribution in the 1st layer for the westerly wind (upper) and easterly wind (lower) cases (thick line indicates 30 psu).

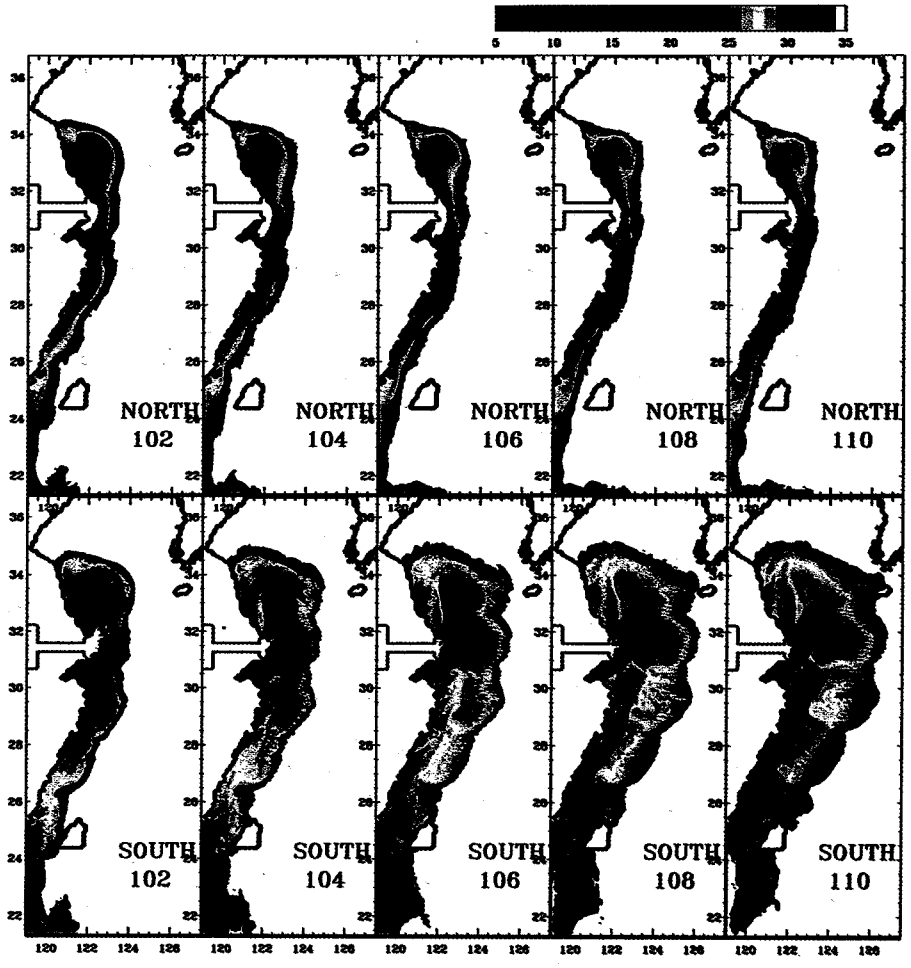

Fig. 9. Same as Fig. 8, but for the northerly and southerly cases.

In the offshore regions where low salinity waters are transported from the west the salinity decreases while in the nearshore regions the salinity increases. The wind effect is not restricted to the redistribution of the low salinity waters. It also affects the discharge from the river. Fig. 11 shows the time series of the discharge for different wind directions. There are more discharge when the wind blows from the south or west than the no wind case and less discharge when the wind blows from the north and east. During the first day when the wind speed increases linearly, the discharge also increases or decreases linearly depending on the wind direction. After the first day the discharge gradually approaches to the magnitude of no wind case. It is expected that the total salinity values over the whole domain would be smaller for the southerly and westerly cases than the northerly and easterly cases because the total discharges are larger in the former.

Vertical salinity distributions in the five east-west sections north of the river mouth starting from the one that crosses the river mouth are shown for the no wind case (Fig. 12) and southerly case (Fig. 13). It clearly shows the effect of the wind on the salinity distribution not only in the horizontal direction but also in the vertical direction. The vertical distribution has a similarity with the observed data of 1996 near the Cheju Island by Kim *et al.* (1998).

Fig. 14 shows the current distribution in the first layer at day 110 in response to the southerly wind. As a direct response to the southerly wind the surface flow is eastward or northward. The coastal current which flows southward when there is no wind now flows to the north and eastward flow is dominant in the offshore region where low salinity waters are transported into. Flow direction near the river mouth is northeastward and the anticyclonic gyre does not exist. Boundary of the flow with appreciable magnitude coincides with the 34 psu isopleths.

Annual variation of river discharge experiment

In this experiment the velocity at the west wall is specified as a sinusoidal form to make the discharge

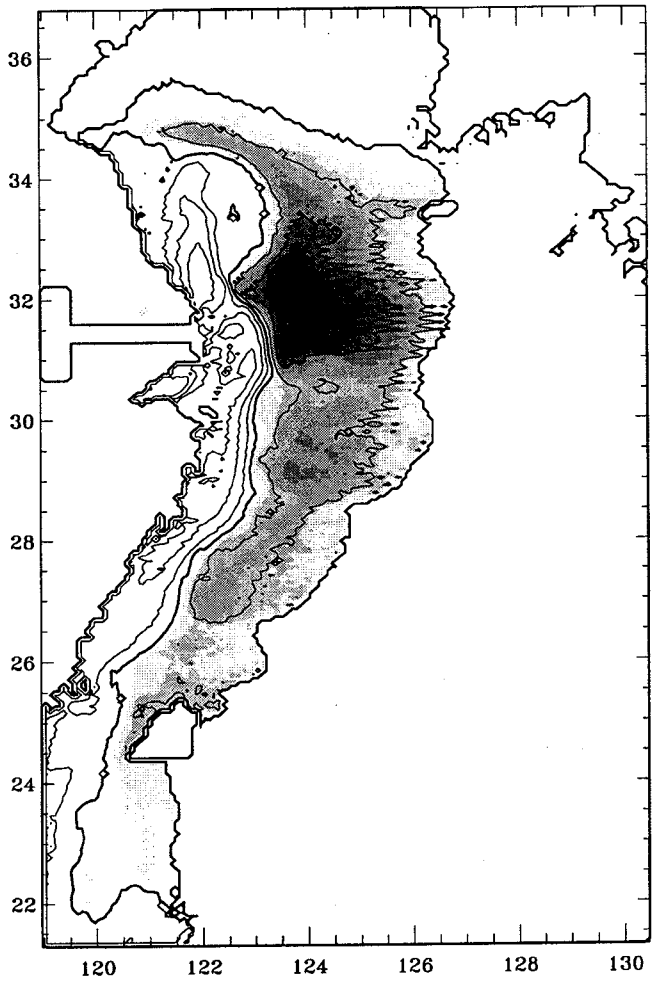

Fig. 10. Salinity changes in the 1st layer due to southerly wind from the no wind case (contour interval is 5 psu and negative values are shaded).

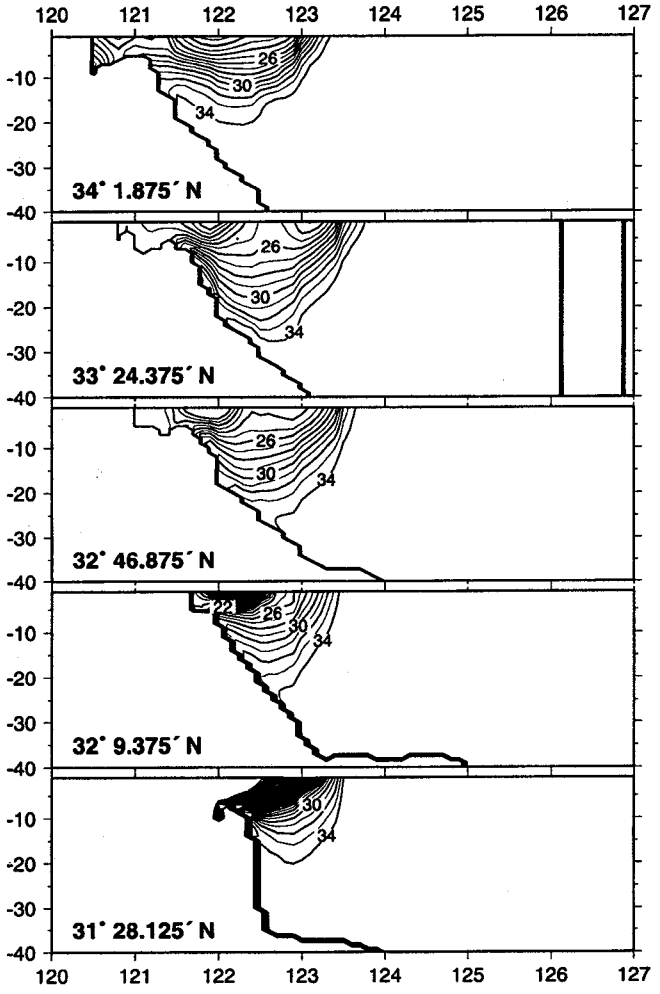

Fig. 12. Salinity distributions in the zonal sections for the no wind case.

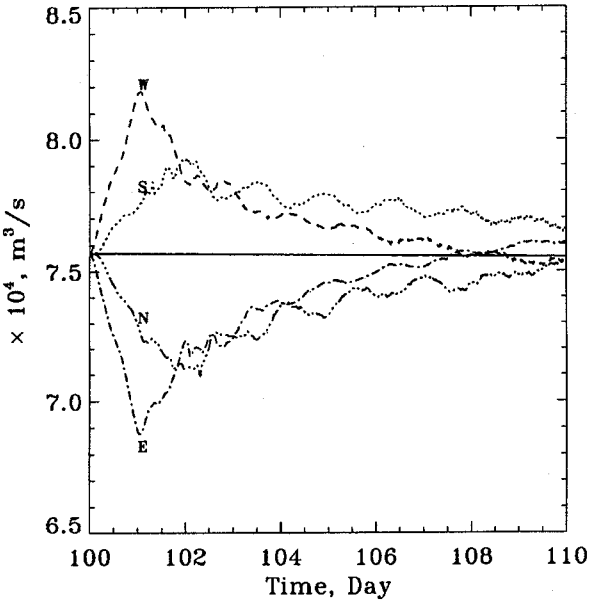

Fig. 11. Time series of the discharge for four different wind directions.

vary with time.

$$U=A\ \sin\left(\frac{2\pi}{360}t+\phi\right)+U_0$$

where

A=3 cm/sec, ϕ=255 days, U_0=4.5 cm/sec

and they are chosen to approximate the time variation of the monthly discharge of Shen *et al.* (1998). The monitored model discharge at the river mouth is shown in Fig. 15. Above values are for the realistic topography case and in the flat bottom case following reduced values are used to take into account the shallow water depth at the river mouth.

A=1 cm/sec, U_0=1.5 cm/sec

The model domain is extended to the north to include the Bohai Sea and the number of y-grid point is now 311. This is because it is expected that the fresh water

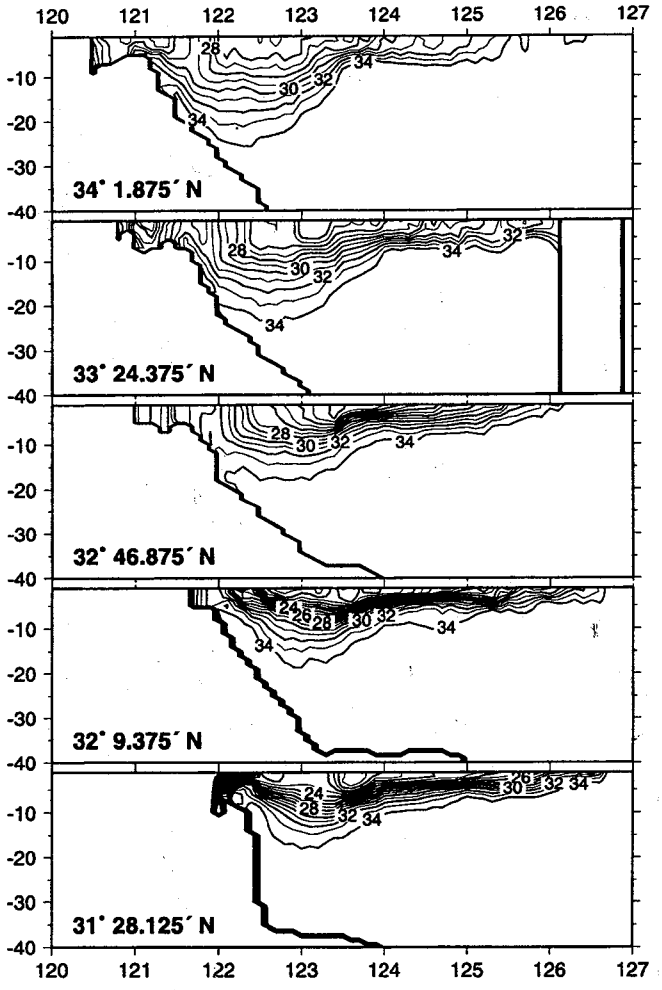

Fig. 13. Same as Fig. 12, but for the southerly case.

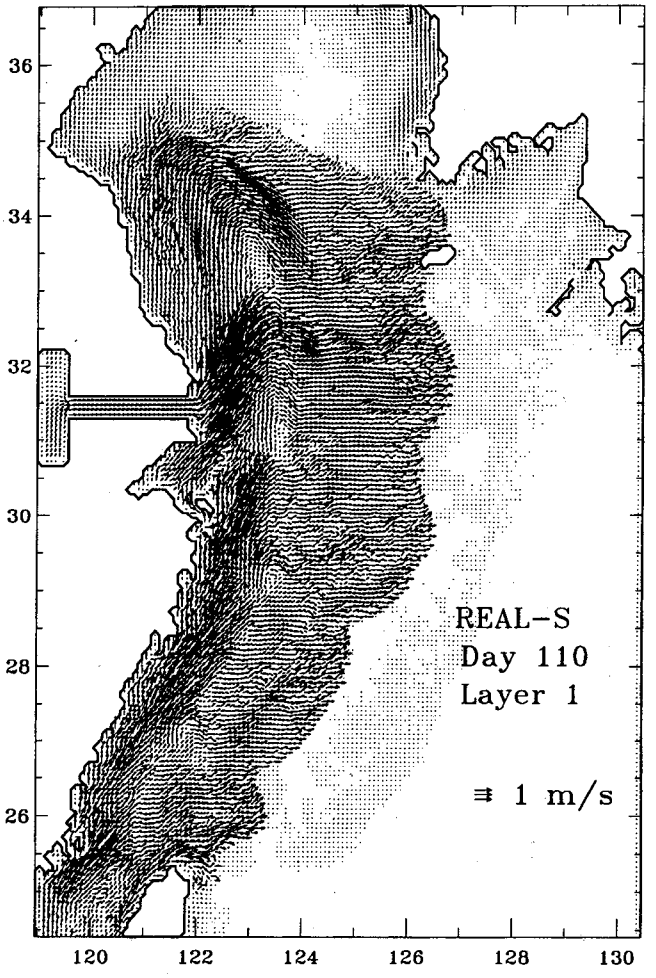

Fig. 14. Velocity distribution in the 1st layer at day 110 for the southerly wind case.

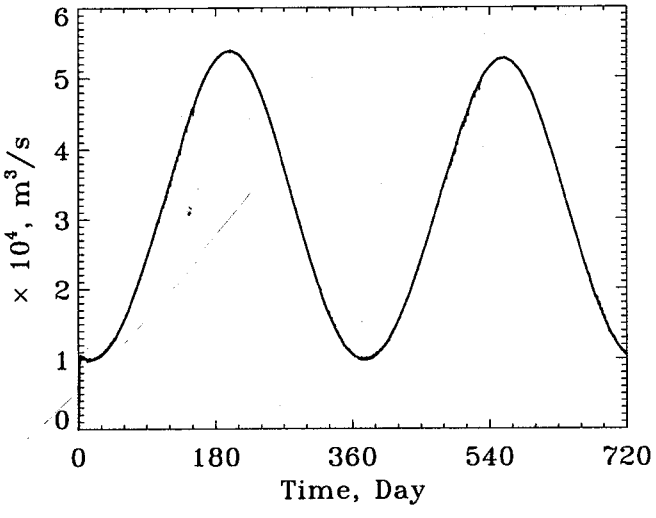

Fig. 15. Annual variation of discharge at the river mouth.

plume will be advected further north than in the previous experiments. Again, flat and realistic bottom cases are tried and the integration is performed for two years (720 days). Salinity distributions in the first layer of the realistic topography case at 60-day interval are shown in Fig. 16. Initial salinity distribution pattern is not much different from the previous experiment but the area is smaller because of the less amount of freshwater discharge. As time goes on the plume becomes larger and at day 120 it reaches the Taiwan Strait to the south and 34°N to the north. The coastal current south of the river mouth reaches the southern boundary at day 160 and the northward plume reaches 35°N at day 200.

After one year (day 360) the plume appears east of Taiwan and the northward plume reaches almost the eastern tip of the Shantung peninsula. In the offshore direction the plume expands to 125°E. The domain of the coastal current is continuously growing to the offshore direction and its width becomes 250 km at day 360. In the second year the northward

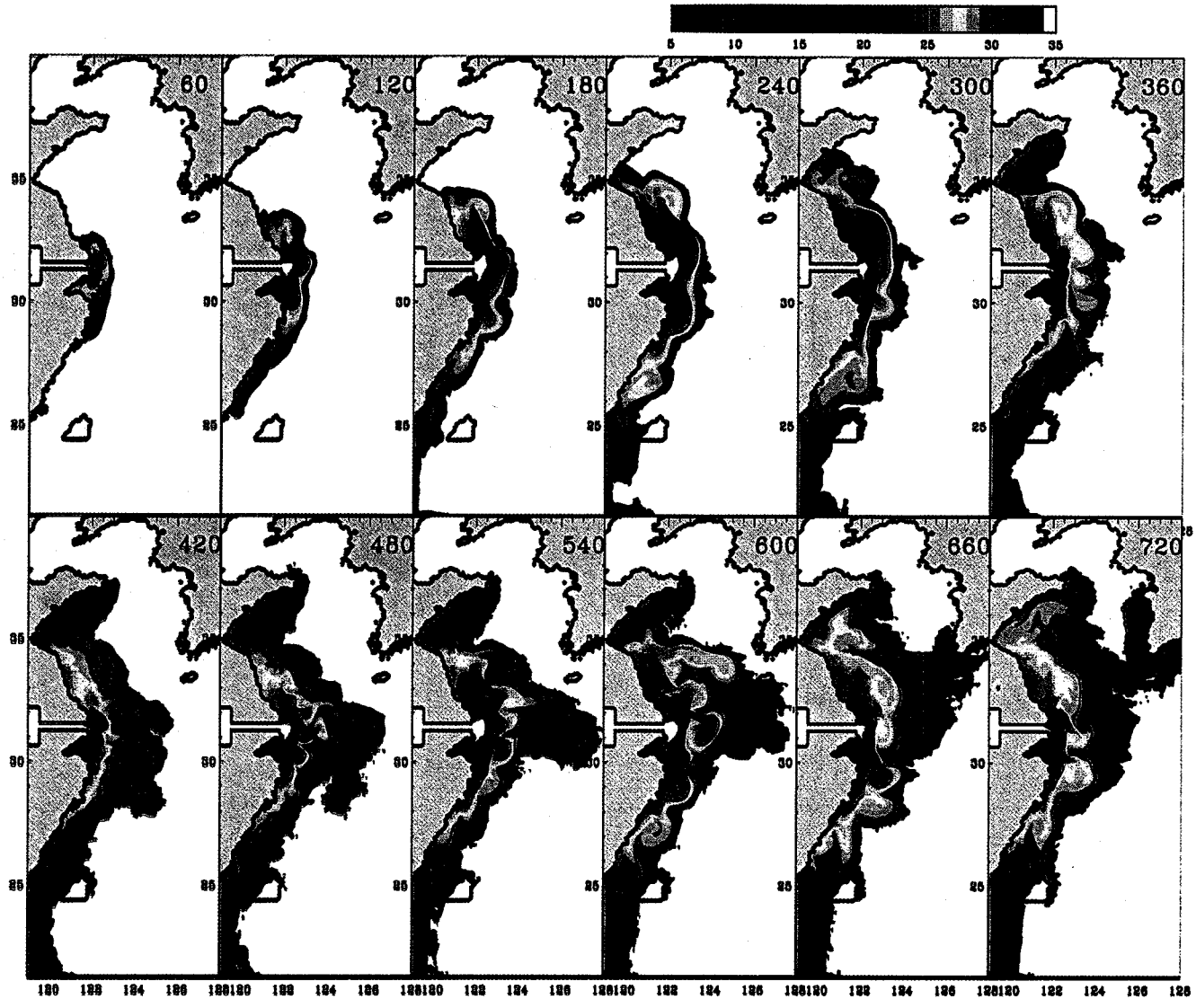

Fig. 16. Salinity distributions in the 1st layer at 60-day interval.

plume reaches the eastern tip of the Shantung peninsula at day 420. It advances westward along the northen coast of the Shantung peninsular until day 480 but soon retreats to the east. The southern plume remains west of 122°E not advancing along the southern wall.

In the central region of 30°—35°N the plume keeps expanding to the offshore direction while the northern and southern plumes are stalling. The main tongue of the plume in the central region is expanding eastward in the southern region of the Cheju Island and reaches 126°E at day 440. At day 500 it passes the longitudes of the Cheju Island and reaches 127°E. Then this tongue is now expanding to the north and reaches the coast of the Cheju Island at day 600. The expansion to the north continues and the whole Cheju Island is surrounded by the low salinity waters at day 640. The plume keeps this northward expansion until it reaches the south and west coasts of Korea. The plume then advances eastward along the south coast and northward along the west coast and at day 720 the plume reaches 129°E in the south coast and 37°N in the west coast.

This experiment is performed to find out the dispersion of the low salinity water by applying only the time-varying discharge without any other external forcing. Therefore the model results cannot be directly compared with the real ocean data. The inclusion of the tide and current would change the whole picture. Nevertheless this experiment shows that the influence of the freshwater from the Changjiang River is large on the ocean environment in the Yellow Sea

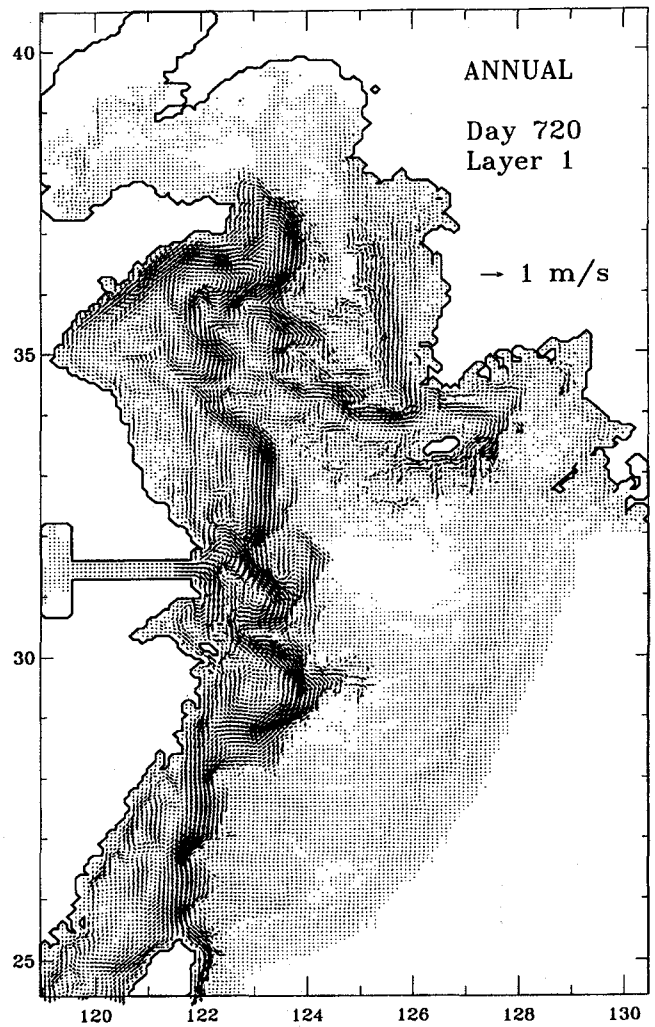

Fig. 17. Velocity distribution in the 1st layer at day 720.

including the South Sea of Korea. In the southern region of the Changjiang River the influence is felt mostly all along near the coast and the offshore expansion is limited to the west of Taiwan. On the other hand the plume expands further offshore in the northen region that the low salinity waters reach not only to the Cheju Island but also to the west and south coasts of Korea. The dispersion of the low salinity waters generates density currents and consequently the ocean circulation would be very complicated. The changes in the ocean circulation would alter the distributions of the chemical/biological parameters and it would lead to the modifications in the ocean ecosystem.

Fig. 17 shows complicated velocity distributions in the first layer at day 720. Strong southward currents are found mostly at offshore locations unlike the first experiment with constant discharge. There exists a northeastward coastal current along the south coast of the Shantung Peninsula and its direction changes clockwise near the eastern tip and then begins to flow southward. Most of this southward current flows through the offshore region all the way to the east of Taiwan. A part of it however flows southeastward toward the Cheju Island until it becomes a northward flowing current at the southwestern corner of Korea. It should be remembered, however, this current pattern is only temporary because the current is a density current induced by the low salinity water which is changing fast in its distribution.

DISCUSSION AND CONCLUSIONS

In this study several experiments are performed under a realistic configuration in the geography and topography. The applied external forcings are designed to be added one by one so that the ocean response to the individual elements could be isolated. In the first experiment the discharge of the Changjiang River is set to a constant value of about 80,000 m^3/s which is, we assume, the same magnitude as in the summer of 1998. Experiments with flat bottom and realistic topography are performed and the introduction of topography reduces the eastward expansion of the plume and enhances the northward flow.

In the second experiment a constant wind is added and we look into the ocean response to the different wind direction. Results confirm that the ocean responds to the applied wind according to the Ekman dynamics and the southerly wind which is the dominant in summer advects the low salinity waters to the east. Therefore the southerly wind alone could be responsible for the appearance of the low salinity waters near the Cheju Island in summer. Certainly, the southerly wind have to be strong enough and/or to last long enough to be effective.

In the third experiment wind is now excluded and a long integration of two years is performed with the time variation in the river discharge. The discharge is designed to change as closely as possible to the monthly discharge data of Shen *et al.* (1998). The experiment starts from a calm and homogeneous ocean and the low salinity water reaches the west and south coasts of Korea in less than two years. The low salinity water occupies the whole Yellow Sea south of the Shantung Peninsula and the resulting density current dominates the circulation.

Anticyclonic gyre and the coastal current along the south coast, an essential feature of the ocean response to the input of the low salinity water, are also present

in our experiments. However, a long integration in the third experiment destroys this basic and simple feature and the structure becomes more complicated. In the basic pattern the outflow from the river flows around the gyre and is connected to the coastal current along the south coast but this simple pattern is no longer possible once the gyre is destroyed by instability or whatever reasons. The flow direction at the river mouth now strongly depends on the local current and this in turn influences the salinity distribution which again changes the current structure. This negative feedback between salinity and current makes the problem very complicated and unpredictable. In other words, the system is predictable when the anticyclonic circular gyre is present but once it is destroyed the system becomes chaotic.

In the realistic topography case of the first experiment more volames of the low salinity waters are advected to the north than in the flat bottom case. The development of the northward flow is also a characteristic feature of the coastally trapped solution of McCreary *et al.* (1997). This feature is explained as a compensating flow induced by the southward flow generated along the density front which is formed offshore between the low salinity river water and the high salinity ocean water. The northward flow in our experiment could be due to the positive relative vorticity associated with the depth increase near the river mouth. The depth increase might be too small to cause this sharp turning, so the dynamics of McCreary *et al.* (1997) looks more responsible for the northward flow.

In this study, simple and idealized external forcings are applied to investigate the behaviors of CRDW in three cases. Thus, we do not attempt to compare the outcomes of this numerical experiments to the real situation. However, our experiments demonstrate that the CRDW can be spreaded significantly in the vast area. Strong tidal current may play a very important role in mixing the freshwater with the saline water in the Changjiang estuary. The Kuroshio system in the East China Sea controls not only the general circulation in the region but also influences the estuarine system. Therefore, tide and the Kuroshio system together with variable winds in time and space should be included to get a closer picture of the real ocean.

ACKNOWLEDGEMENTS

This study was supported partly by the Korean Ministry of Maritime Affairs and Fisheries.

REFERENCES

Kim, S.S., W.J. Go, Y.J. Jo, P.Y. Lee and K.A. Jeon, 1998. Low salinity anomaly and nutrient distribution at surface waters of the South Sea of Korea during 1996 summer. *The Sea, J. Korean Soc. Oceanogr.*, **3**: 165 – 169.

Cao, X., 1980. The numerical model of the summer surface salinity distribution of the Changjiang Diluted Water (in Chinese). *Acta Oceanologica Sinica*, **2**: 1 – 6.

Chao, S.Y., 1988. River-forced estuarine plumes. *J. Phys. Oceanogr.*, **18**: 72 – 88.

Guan, B., 1994. Patterns and structures of the currents in Bohai, Huanghai, and East China Seas. In: Oceanology of China Seas, Vol. 1, edited by D. Zhou, Y.B. Liang and C.K. Zeng, Kluwer Academic Publishers, Dordrecht, pp. 17 –26.

Hong, G.H., S.H. Kim, C.S. Chung and S.J. Pae, 1995. The role of the anthropogenic nutrient input in the carbon fixation of the coastal ocean Yellow Sea: a preliminary study. In: Direct Ocean Disposal of Carbon Dioxide, edited by N. Handa and T. Ohsumi, Terra Scientific Publishing Company, Tokyo, pp 13 – 22.

Hu, D., 1994. Some striking features of circulation in Huanghai Sea and East China Sea. In: Oceanology of China Seas, Vol. 1, edited by D. Zhou, Y.B. Liang and C.K. Zeng, Kluwer Academic Publishers, Dordrecht, Netherlands, pp. 27 – 38.

Kangshan, W., S. Jilan and D. Lixian, 1983. Hydrographic features of the Changjiang Estuary. In: Sedimentation on the Continental Shelf, With Special Reference to the East China Sea, Vol. 1, edited by Acta Oceanologica Sinica, China Ocean Press, Beijing, China, pp. 137–147.

KORDI, 1997a. Ocean circulation and material flux of the East China Sea -Eastern East China Sea-. KORDI Report, BSPN 00319-964-1, 563 pp.

KORDI, 1997b. A numerical modeling study of the Yangtze River Diluted Water. KORDI Report, BSPE 97616-00-1056-1, 69 pp.

Lie, H.J., C.H. Cho, J.H. Lee, P. Niiler and J.H. Hu, 1998. Separation of the Kuroshio water and its penetration onto the continental shelf west of Kyushu. *J. Geophys. Res.*, **103**: 2963 – 2976.

Lee, D.E., 1999. Three-dimensional modeling of the circulation in the Yellow and the East China Seas. M.S. Thesis, Seoul National University, Seoul, Korea, 102 pp.

Lee, H.C., 1996. A numerical simulation for the water masses and circulations of the Yellow Sea and the East China Sea. Ph.D. Thesis, Kyushu university, Fukuoka, Kyushu, Japan, 150 pp.

Mao, H., Y. Ren and G. Sun, 1963. A preliminary study of the Yangtze Diluted Water and its mixing process (in Chinese). *Oceanologia et Limnologia Sinica*, **5**: 183 – 206.

McCreary, J.P. Jr., S. Zhang, and S.R. Shetye, 1997. Coastal circulation driven by river outflow in a variable-density 1-layer model. *J. Geophys. Res.*, **102**: 15535 – 15554.

Mellor, G.L., 1996. Users guide for a three-dimensional, primitive equation, numerical ocean model. Atmospheric and Oceanic Sciences Program, Princeton University, Princeton, 40 pp.

Mellor, G.L. and T. Yamada, 1982. Development of a turbulence closure model for geophysical fluid problems. *Rev. Geophys. Space Phys.*, **20**: 851 – 875.

Oey, L.Y. and G.L. Mellor, 1993. Subtidal variability of estuarine outflow, plume, and coastal current: a model study. *J. Phys. Oceanogr.*, **23**; 164 – 171.

Shen, H., C. Zhang, C. Xiao and J. Zhu, 1998. Change of the dis-

charge and sediment flux to estuary in Changjiang River. In: Health of The Yellow Sea, edited by G.H. Hong, J. Zhang and B.K. Park, The Earth Love Publication Association, Seoul, pp. 129 – 148.

Yuan, Y. and J. Su, 1984. Numerical modelling of the circulation in the East China Sea. In: Ocean Hydrodynamics of the Japan and East China Seas, edited by T. Ichiye, Elsevier, Amsterdam, Netherlands, pp. 167 – 186.

Yuan, Y., J. Su and J. Zhao, 1982. A single layer model of the continental shelf circulation in the East China Sea. *La mer*, **20**: 131 – 135.

Zhu, J. and H. Shen, 1996. The mechanism of the expansion of the Changjiang (Yangtze River) Diluted Water. East China Normal University Press, Shanghai, China, 255 pp.

Manuscript received May 6, 1999
Revision accepted September 20, 1999